



HAL
open science

From microwave gas sensor conditioning to ammonia concentration prediction by machine learning

Alexis Lasserre, Ludmilla Grzelak, Jérôme Rossignol, Olivier Brousse, Didier Stuerga, Michel Paindavoine

► **To cite this version:**

Alexis Lasserre, Ludmilla Grzelak, Jérôme Rossignol, Olivier Brousse, Didier Stuerga, et al.. From microwave gas sensor conditioning to ammonia concentration prediction by machine learning. *Sensors and Actuators B: Chemical*, 2022, 367, pp.132138. 10.1016/j.snb.2022.132138 . hal-04024398

HAL Id: hal-04024398

<https://hal.science/hal-04024398>

Submitted on 22 Jul 2024

HAL is a multi-disciplinary open access archive for the deposit and dissemination of scientific research documents, whether they are published or not. The documents may come from teaching and research institutions in France or abroad, or from public or private research centers.

L'archive ouverte pluridisciplinaire **HAL**, est destinée au dépôt et à la diffusion de documents scientifiques de niveau recherche, publiés ou non, émanant des établissements d'enseignement et de recherche français ou étrangers, des laboratoires publics ou privés.



Distributed under a Creative Commons Attribution - NonCommercial 4.0 International License

From microwave gas sensor conditioning to ammonia concentration prediction by machine learning

Alexis Lasserre ^a, Ludmilla Grzelak ^{a,b}, Jerome Rossignol ^a, Olivier Brousse ^b, Didier Stuerga ^a, Michel Paindavoine ^b

^a GERM, Dept Interfaces, Laboratoire Interdisciplinaire Carnot de Bourgogne, UMR CNRS 6303, UBFC, Dijon, France

^b Yumain, Dijon, France

Abstract

This paper proposes an innovative approach to understand the conditioning process of a microwave gas sensor operating at room temperature based on the combination of its response and the interpretation of the mass spectrometer data. A large variation of the dielectric parameters and thus of the microwave response is due to water departure from the sensor surface. Consequently, the first step of the conditioning process is a carrier gas sweep of the sensor surface. The second step consists in pre-saturating the microwave gas sensor surface with a high concentration of the polluting gas which will be detected (here ammonia). This process results in a very good quality microwave response on the qualitative and quantitative aspects for the detection of ammonia in the air and is helping the work carried out in this article in artificial intelligence on microwave responses. A regressor machine learning model is applied on time samples of this sensor response to predict the ammonia concentration. Several machine learning algorithms are tested and compared. Principal Component Analysis is also tested to reduce the input data dimension, but results are not conclusive. The concentration profile is revised to reduce the bias induced by the presence of too much measurement data when no pollutant is present in the air. And the Multi-Layer Perceptron regressor gives the best results with a mean absolute error of 32.13 ppm (8%) over a range of 0 to 400 ppm and R-squared score of 0.87.

Keywords: microwave gas sensor, mass spectrometry, ammonia, deep learning, conditioning process

1 Introduction

Ammonia is a gaseous pollutant whose atmospheric concentration varies greatly with human activity such as industrial or agricultural processes (explosives, fertilizers, polymers, fuel cells, etc.) [1]. Ammonia can have short- and long-term health effects on both humans and animals, hence the need to detect it effectively in real time in the atmosphere [2,3]. It is also responsible for forming fine particles and for the eutrophication of water [4–7]. Although microwave transduction is less mature (~ 20 years) than conventional transductions, several applications have been demonstrated such as humidity detection, detection of polluting gases or an analyte in a liquid phase [8–10]. This consists of a microwave resonator, coated with a sensitive material (either insulators or conductors) whose electromagnetic properties vary in the presence of gas [11–13]. However, it allows real-time detection of gases at room temperature over a wide concentration range and is convenient for the world of the Internet of Things since it requires the electronics already present in the radio frequency signal transmission technology [14–17]. Previous works highlight that the microwave gas sensor has a similar behavior whatever the carrier gas, towards the detection of ammonia in a frequency range from 1 to 8 GHz [18]. Recently J. Rossignol et al. have shown through a comparative study the influence of the manufacturing process and deposition of the sensitive material on a microwave sensor for ammonia detection, as well as the influence of the dielectric properties of the sensitive layer [19]. The performance of the microwave gas sensor presented in this work is to be put in perspective with other microwave ammonia sensors found in the

literature. Reiß et al. and Bogner et al. present a sensor capable of measuring ammonia concentrations of 500 and 1000 ppm. Jun et al. demonstrate the detection efficiency of their gas sensor in the range of 0.1 to 1 ppm. Thus, the sensor that is proposed in this paper falls between the two ranges already described in the literature with a possibility of continuous detection in the range 10 - 400 ppm of ammonia which highlights its versatility [20–22]. The innovative aspect of this presented work comes from the real-time monitoring of gases present in the cell thanks to microwave gas sensor in combination with the mass spectrometer (MS). The use of this chemical analysis tool helps to prove the link between the variations of the chemical composition of the gas phase and the variations of the observed microwave signal. Indeed, connected directly to the cell outlet, the MS provides real-time qualitative and quantitative analysis of the composition of the gas phase present inside the cell by separating species according to their mass (m/z).

There are few papers on the observation and interpretation of "memory effects" of gas sensors. However, Vasiliev et al. observed a cumulative behavior of the ammonia gas sensor after successive exposures [23]. This effect leads to the creation of an interface electric field resulting from the adsorption of polar target species. The cancellation of the accumulation, direct manifestation of the memory effect, is done by applying a reverse polarization on the junction causing a desorption of the species. Bendahan et al. showed the need for prior exposure of the gas sensor to the target (ammonia) to ensure a reversible and quantitative response in a second step [24]. In their work, this exposure is justified by the extreme affinity between the target (ammonia), and the substrate (CuBr) leading to a mixed species $[\text{Cu}(\text{NH}_3)_2]^+$. Based on the experimental analyses in this work, a proposal for a reasoned conditioning protocol is described in this article. This protocol is a continuation of the work mentioned above in order to obtain the same consequences (a qualitative and quantitative measurement) but for different causes (adsorption mechanisms and microwave transduction).

Other detection work has already been carried out using a MS, notably for the analysis of inhaled gas or body odor for the detection of diseases or the quality of foodstuffs such as the rancidity of potatoes or blueberries [25–29]. Unlike other conventional transductions, MS monitoring of the experiments has not yet been implemented to assess the characteristics of microwave transduction and its ability to be selective. Another advantage of using a MS is the accurate tracking of water, which is a major interferent in atmospheric detection.

One aim of this paper is being able to determine for each time sample of a manipulation a range of pollutant concentration, here ammonia. To achieve it regression models of machine learning (ML) are implemented. In the literature, research has been done to obtain quantitative results with arrays of gas sensors and the help of machine learning models for different types of applications [30–36]. But it has never been done using a single microwave gas sensor. The ML models presented here are applied on time samples. Models classically used like Principal Component Analysis (PCA) combined or not with either Support Vector Regression (SVR), k-Nearest Neighbors (k-NN), Random Forest (RdmF), Linear Regressor (LR) or Multi-Layer Perceptron (MLP) and some others like Convolutional Neural Networks (CNN) are tested and compared in this article.

2 Material and methods

2.1 Experimental set-up and microwave gas sensor

The generation of dry gases (air, air + ammonia) is done by conventional calibrated Air Liquide gas cylinders (water concentration < 3 ppm). The gas flows are managed by Bronkhorst EL-Flow select F-201CV mass flow controllers (MFC). The change from one gas to another is done by means of a pneumatic valve. The cell used is an all-glass cell to reduce all coadsorption phenomena to a minimum. Microwave response is collected by a Rohde Schwarz R&S ZVB Vector Network Analyzer (VNA) scanning over a range from 10 MHz to

8 GHz (5001 sweep number). The time required for the VNA to acquire all the spectrum microwave data over the working frequency range, also known as sweep time, is 10 seconds for the whole process. LabView's acquisition of the experimental data occurs once every 20 seconds. A Rotronic HC2-S humidity and temperature sensor is installed at the end of the set up to track these parameters during the experiments. The gas sensor operates at room temperature ($22\text{ }^{\circ}\text{C} \pm 1$). The whole set up is controlled by LabView® on a dedicated computer. When no experiment is in progress, the cell and the sensor are in direct contact with the outside atmosphere. The schematic of the experimental set up is specified in the appendix section (Fig. A.1).

The design of the used microwave gas sensor is based on a spiral microstrip with 6 resonant frequencies uniformly distributed in the 2 to 8 GHz range. These frequencies are not harmonics but resonance frequencies that are directly related to the number of coils in the sensor structure) [37]. The complete structure of the sensor and its dimensions can be found in the appendix section (Fig. A.2). The substrate is Duroid® 6202 with a relative permittivity $\epsilon_r = 2.94$. The superstrate is a patch of sensitive material AEROXIDE® TiO₂ P 25 from Evonik prepared in water and deposited by doctor blade on the spiral area.

The choice of a very low relative permittivity substrate and the use of a titanium dioxide layer with a high relative permittivity aims at maximizing the radiation of the spiral. The description of these resonant frequencies over the range 1 to 8 GHz is proposed in a previous paper as well as the influence of the sensitive material deposition on the resonant frequencies. It has been shown that the TiO₂ patch shifts the resonance frequencies downwards (i.e 230 MHz shift at 3 GHz) [37]. The relative permittivity of the TiO₂ P25 from Evonik layer was evaluated at $\epsilon_r = 6.4 \pm 0.1$ [19].

2.2 Mass spectrometer monitoring and water detection

Ammonia ($m/z = 17$) and water ($m/z = 18$) form fragments with very close masses. HIDEN HPR20 mass spectrometer allows the user to assign to each analyzed mass its own ionization energy in the range 0 to 150 eV by increment of 0.1 eV. The ionization of water is minimal below an energy of 15 eV. Indeed, the ionization of H₂O into H₂O⁺ occurs from 15 eV and beyond 20 eV H₂O ionizes into OH⁺. However, the ionization energy of NH₃ into NH₃⁺ is 11 eV which implies that there is a threshold from which we can observe an effective ionization of ammonia without it impacting water [38,39]. So, an ionization energy of 15 eV for ammonia is chosen to effectively separate ammonia from water. In the following, pressure variations are tracked by the MS during the experiment. VNA and the MS measurements are synchronized.

2.3 Data preparation

The MS placed at the end of the experimental bench is a reliable reference for the monitoring of ammonia in the air and provides, once calibrated, the ammonia concentration in the presence of the sensor. Thus, its response is used as ground truth to label the input data for the supervised machine learning models used. Depending on the experimentation, different sensors have been used [19]. Since the thickness of the deposited layer of sensitive material on the sensor can vary as well as the calibration of the VNA and the history of the sensor (initial humidity, number of cycles to which it has already been exposed, etc.) an offset is present on the S₁₁ data. The processing of microwave data can be done in two ways: a study of the time variations of the magnitude and phase at a fixed frequency or a study of the time variations of the resonance frequency. In this article, results from both approaches will be used. [16,19]. To reduce the offset, the magnitude and phase response are normalized against the value obtained just before the first injection of pollutant. This chosen value corresponds to a time where there is no pollutant, and the water concentration is stable and reached its minimum.

2.4 Feature selection

Since the microwave response (S_{11}) provide a large data vector for each time sample (5001×2), a reduction of the vector dimension is performed. For this, only the most relevant data are kept, this is the feature selection. Two feature selection methods are implemented and compared in this paper: a manual selection of features around the resonant frequencies and a feature selection using Pearson's correlation coefficients.

2.4.1 Manual selection

As the designed microwave gas sensors has 5 to 6 observable resonant frequencies depending on the set frequency comb on the VNA and as the sensor is more sensitive around these frequencies a focus is made on them (Fig. 1). For each type of response (magnitude and phase) a selection of the 100 features present around each resonant frequency is done. This reduces the input data to a vector of 500 or 600 features (depending on the resonant frequencies available) per type of response.

2.4.2 Pearson's correlation

Pearson's correlation coefficient gives the correlation between two data [40]. A calculation of the coefficient of each feature against the ammonia concentration is done. To make the two feature selections comparable, the same number of features are selected in both of them. The models presented below take a simple input vector, the obtained frequency windows are concatenated as well as the corresponding magnitude and phase vectors. This gives an input of dimension (1000×1) or (1200×1) depending on the frequency range.

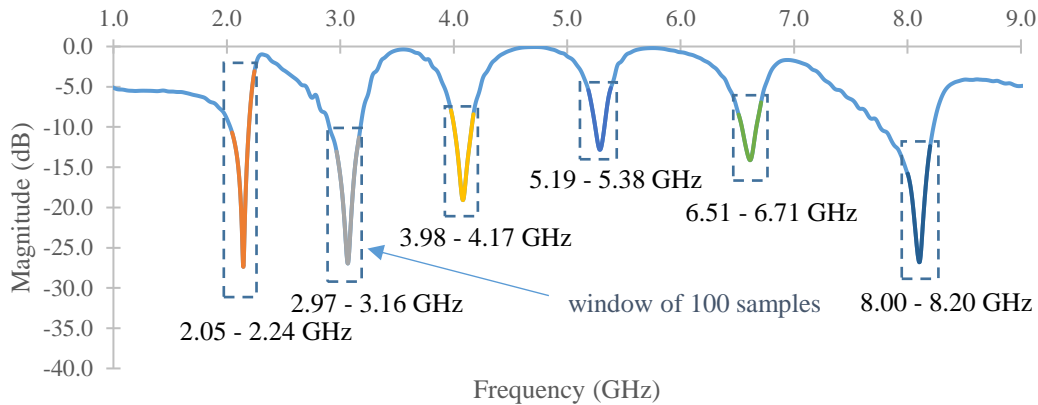


Fig. 1. Example of S_{11} magnitude vs frequency for one sensor and its segmentation to get 100 samples windows around resonant frequencies.

2.4.3 Principal Component Analysis

In addition to any of the feature selections and in order to further reduce the data size a PCA is implemented. In order to better understand the impact of the PCA on the results the results with and without PCA are presented in this paper. PCA has been implemented for all models except the CNN which has its own feature extraction.

PCA finds linear combinations called principal components and projects data on a lower-dimensional space by choosing axes keeping the maximum of the data initial variance [41]. To determine the number of needed components a threshold is set, 99% in this paper, and PCA stops when the first n components account for a percentage of total variation greater than this threshold.

2.5 Machine learning (ML) models

To predict the ammonia concentration from the microwave sensor response different regressors models are implemented and compared.

Different ML models are used in the literature for the classification or prediction of gas concentration in the air from a combination of sensors [30–36]. Using a single microwave gas sensor can be similar to using multiple sensors at the same time because this type of sensor returns a dual response for each frequency of its comb. This is why the use of this type of ML models and their comparison is made in this article.

2.5.1 *Classical machine learning models*

The most classically used machine learning algorithms for gas sensors are SVM [42], k-NN [43] and RdmF [44]. Here, as it is a regression that is to be implemented, it seems important to compare the results of the three models mentioned with another very classical regression model which is linear regression.

LR is a linear model, it determines, using the least squares method, the linear equation that gives the minimum error for the given dataset [45]. Support Vector Machine (SVM) is one of the most influential approaches to supervised learning. SVM is mostly used for classification but a version for regression called SVR will be used here [46,47]. SVM divides the feature space by finding the support vectors with the highest distance between the nearest points of each class. SVR uses the same principle as SVM but applied to regression problems. The k-NN finds the input k nearest neighbors within the stored trained dataset as per the calculated Euclidean distance and averages their labeled values. The number of neighbors giving the best score is used. RdmF is an ensemble method. It combines the predictions of multiple decision trees into a single model to reduce the possibility of overfitting. RdmF are known to be a traditional model that can compete with Artificial Neural Networks (ANN) especially because it is less computationally expensive and can work with less data.

2.5.2 *Multi-Layer Perceptron*

To compare these models with ANN a MLP regressor with fully connected neurons is implemented. It is small but robust, has a hidden layer of 100 neurons, uses the Rectified Linear Unit (ReLU) activation function for its hidden layer and the identity one for the output. Adam optimizer is used [48].

2.5.3 *Convolutional neural network*

The CNN uses a mean squared error loss function and an Adam optimizer. A CNN is composed of two complementary parts: feature extraction and pattern recognition. The CNN feature extraction part consists here of a one-dimension (1-D) convolution layer of 128 neurons with ReLU activation function followed by a dropout layer to prevent overfitting. This convolution layer will take the input vector and apply a convolution filter of kernel size 3. As the magnitude or the phase are associated with a frequency, the filter will convolve neighboring frequency responses and extract features. A flattening layer is used to link the two parts, it converts the data into a 1-dimensional array so that a Fully Connected (FC) layer can take it as an input. As for pattern recognition it is done with a FC layer of 64 neurons tailed by the output layer. The FC layer uses a ReLU activation function and the output layer a linear one.

2.6 *Used metrics to compare the regressions models*

Classify the metrics used to analyze the regressors performances are the mean square error (MSE) and its rooted variant (RMSE), or the mean absolute error (MAE) [49]. Their interpretation depends on the type of prediction values because they can be between zero and infinity. As for the coefficient of determination (R-squared or R^2), it is a statistical measure of how well the regression predictions approximate the real data points. It is not lower bound but an R^2 of 1 indicates that the regression predictions perfectly fit the data and a negative value means the regressor performed poorly [50]. Chicco et al determined that R^2 is more informative than MAE, MSE and RMSE in regression analysis evaluation and recommend standardizing its usage [50]. That is why to interpret the results of the regressors presented in

this article a focus is made on the R^2 score. However, to differentiate models with close R^2 scores MAE is used.

3 Results and Discussion

3.1 Influence of water on the microwave response

Water is a major interferent in the detection of pollutants in air. The behaviors of the sensor are analogous on the analyzed frequency range, but the variations are more or less important according to the chosen resonance frequency. Here, 4.93 GHz is chosen because this resonance presents a significant variation in magnitude. The magnitude variations of the microwave signal at 4.93 GHz as a function of time is represented in orange in Fig. 2. The partial pressure of the mass fragment $m/z = 18$ as a function of time is in blue.

The water presence in the beginning of each experiment is firstly explained by the fact that the sensor is deliberately in contact with atmospheric air. Moreover, if it is the first use of the sensor, its surface is saturated with water since the deposition of sensitive material is done using water as a solvent. At the beginning of the experiment, the cell is exposed to dry air at 0.5 L/min for over an hour. It can be observed in Fig. 2 that the partial pressure related to mass fragment $m/z = 18$ decreases dramatically over the first few minutes because of the replacement of the humid atmospheric air by the dry air of the gas cylinder. The water departure has a huge influence on the microwave signal since a strong decrease of the signal magnitude following the water departure is observed. The two variations are almost superimposed. The criterion chosen to determine the efficiency of the cleaning of the sensor surface is experimental and is provided by the MS. Indeed, when the variations of the mass fragment $m/z = 18$ stabilize, i.e., when the water outflow stabilizes, then the magnitude of the microwave signal also stabilizes.

Therefore, it is important to control the water departure to have a good quality microwave response both qualitatively and quantitatively. This process is the first step of the conditioning process of the gas sensor.

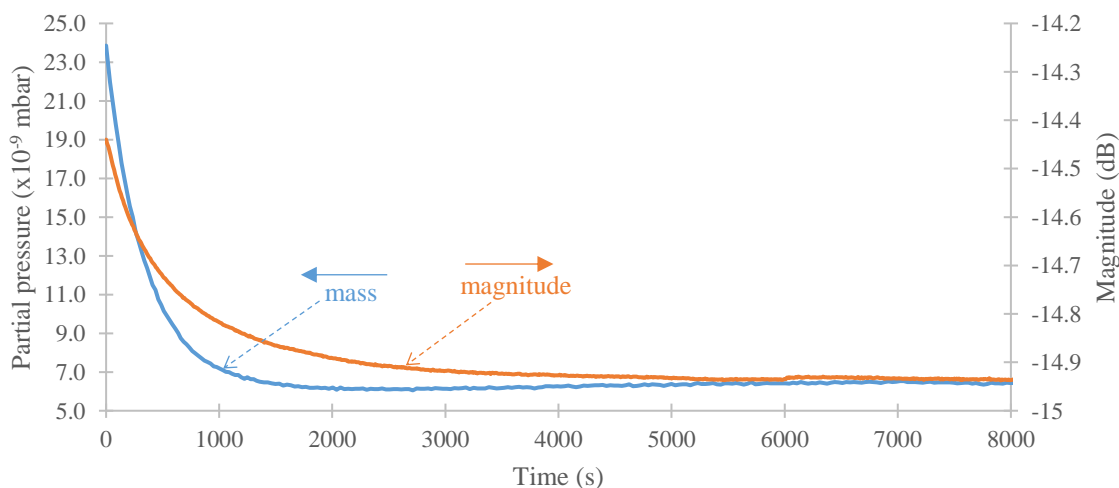


Fig. 2: Partial pressure of mass fragment $m/z = 18$ (blue) and magnitude (orange) at resonant frequency (4.93 GHz) vs time.

3.2 Qualitative and quantitative aspects of microwave gas sensor response

The first part of this work shows the primordial role of the carrier gas sweep that must be performed before each experiment. Carrier gas sweeping allows the departure of water but, more generally, constitutes a cleaning phase of the surface of the gas sensor. Fig. 3 shows as an example the maximal magnitude variation of the microwave sensor at 5.97 GHz, in orange, as a function of time as well as the time tracking of the partial pressure of mass fragment m/z

= 17, in blue, attributed to an ionized fragment of ammonia. This figure shows that the magnitude variations of the microwave sensor is directly correlated to the variations of the mass fragment $m/z = 17$, thus to the presence or absence of ammonia. The consistency of the microwave response with respect to the pollutant is shown here. The curve indicates that the microwave signal and the mass tracking are superimposed, which demonstrates that the sensor sends back real time information from the atmosphere, qualitatively the sensor acts as a mirror of the atmosphere.

However, this is not enough to get a good microwave signal quality. Indeed, empirically, it has been noticed that the first pulse of pollutant gas concentration following the departure of water were almost systematically overestimated compared to what was expected. However, it is observed that the microwave response to the first NH_3 pulses (between $t = 2700\text{s}$ and $t = 6000\text{s}$) is almost identical in amplitude whatever the concentration. The concentration being directly linked to the partial pressure of the fragment $m/z = 17$ measured by the MS. This reflects a non-quantitative response of the sensor to the pollutant gas solicitation. So, it was decided to integrate an ammonia pulse, called "conditioning pulse", into the conditioning process to favorize the saturation of the sensitive surface. The aim is to put the gas sensor in contact with a high concentration of ammonia (typically 400 ppm) for at least 30 minutes just after the water departure. Indeed, when a target to be detected (here ammonia) is put in contact with a surface considered as cleaned, i.e. never having been in contact with this target, two phenomena come into play. A part of the target is strongly adsorbed at a very short distance from the surface by creating a chemical bond (chemisorption) and giving rise to a phenomenon of hysteresis which requires a significant energy input if this phenomenon is to be reversed. In the case of the presented sensor, since it is covered with a layer of nanostructured sensitive material, this effect is even more reinforced. The other part of the target is in much weaker interaction with the surface and can thus desorb much more easily without significant energy input (physisorption).

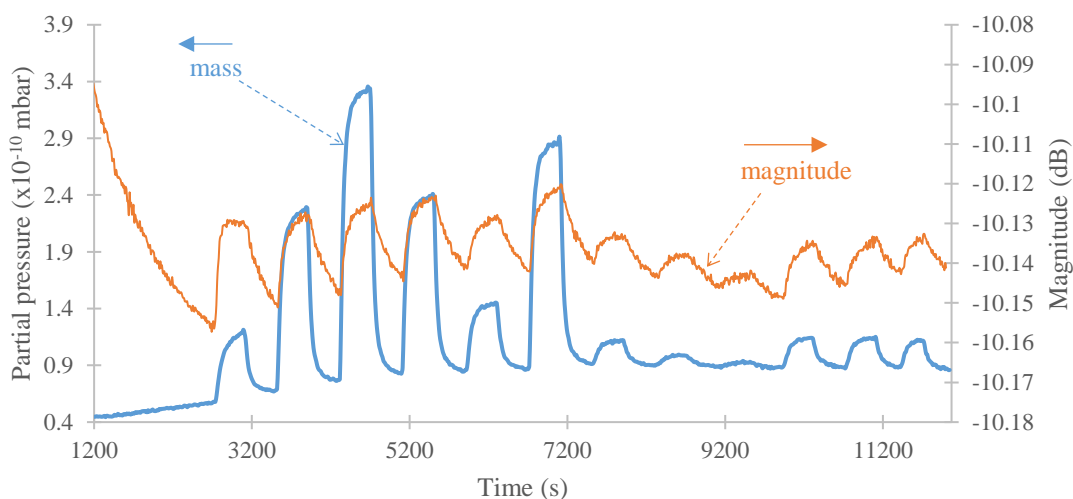


Fig. 3: Magnitude at a resonant frequency (5.97 GHz, orange) and partial pressure of mass fragment $m/z = 17$ (blue) vs time, obtained by MS, without conditioning pulse.

Therefore, the main hypothesis to explain the necessity of this second step in the conditioning process would be that this "conditioning pulse" would result in a pre-saturation of the surface adsorption sites. This "conditioning pulse" satisfies the conditions of chemisorption and what we observe afterwards is physisorption which would also explain the speed with which the gas sensor detects the pollutant [51].

Then, the proposed conditioning cycle is composed of a sweep with carrier gas for at least 1 hour followed by a conditioning pulse at high concentration of the pollutant gas to be

detected, typically 30 min at 400 ppm for ammonia followed by another sweep of carrier gas for several tens of minutes. The results presented below (in magnitude and frequency) were preceded by the conditioning cycle described.

Fig. 4 shows the magnitude variations of the microwave signal at 4.93 GHz, in orange, and the partial pressure of mass fragment $m/z = 17$ as function of time, in blue are. This figure illustrates the qualitative and quantitative behavior of the microwave gas sensor obtained after the conditioning process. Indeed, the magnitude variations are greater when the sensor is subjected to a higher concentration of ammonia. This result is coherent with the partial pressures of the fragment $m/z = 17$ measured by the mass spectrometer, and which are related to the concentration. It should be noted that this conditioning does not exclude the presence of a drift on the baseline, but the use of ML models makes it possible to ignore it. The monitoring of pressure during the experiment in the cell eliminates any assumption of over pressure (overshoot) at the time of concentration changes. The temperature monitoring highlights a one-degree Celsius variation for all experiments. Where usually the hypotheses to explain the drifts turn to physical parameters such as a thermal drift during the experiments, the contribution of the MS here allows the formulation of a purely chemical hypothesis for the explanation of this drift.

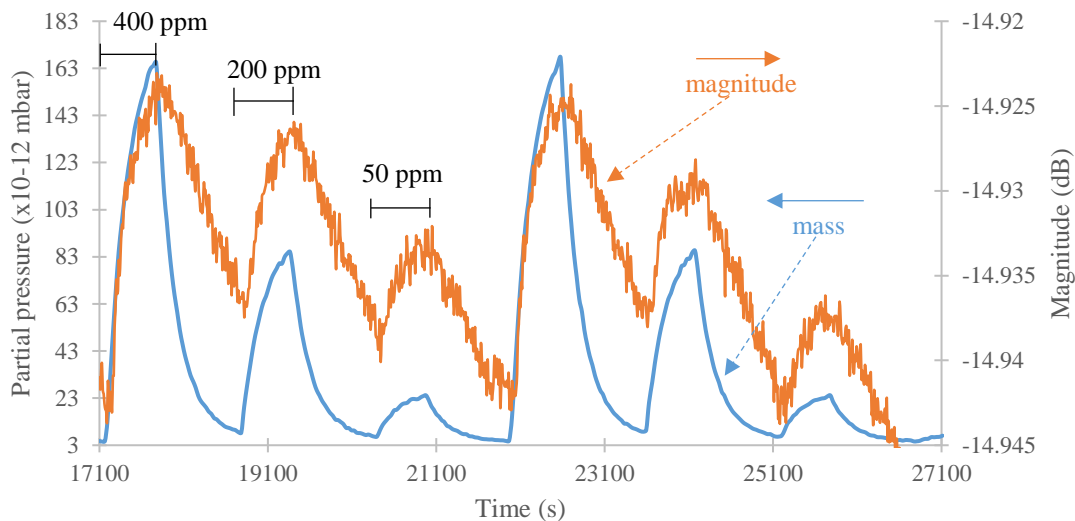


Fig. 4: Partial pressure of mass fragment $m/z = 17$ (blue) and magnitude (orange) at resonant frequency (4.93 GHz) vs time. Estimated drift slope: 0.012 dB/h.

The qualitative and quantitative aspect of the microwave sensor response was also demonstrated for lower concentrations with ammonia pulses ranging from 10 to 50 ppm and the results are presented in the appendix section (Fig. A.4). Regarding detection at lower concentrations, work is underway to lower the detection threshold and optimize the signal-to-noise ratio. Similarly, the work presented can also be done on the resonant frequency shift. Fig. 5 shows the frequency shift vs time. Depending on the frequency at which the analysis is performed, frequency shifts of a few MHz to several tens of MHz are observable for the water departure in the first minutes of the experiment. The most significant frequency shifts were observed at 5.29 GHz. Analogous to the variation of the magnitude response, it is observed that the departure of water causes a big shift of the resonance frequency. Indeed, this big frequency shift is explained by the fact that the departure of water implies a decrease of the dielectric permittivity thus an increase of the resonance frequency. This phenomenon is observed between $t = 0$ s and $t = 6600$ s. On the other hand, the introduction of ammonia for the conditioning pulse from $t = 6600$ s to $t = 8400$ s causes a decrease in the resonance

frequency. Unlike the water desorption, here the adsorption of ammonia implies the increase of the dielectric permittivity and thus the decrease of the resonance frequency. It is a typical behavior of adsorption and desorption of a gas species on the surface of a microwave gas sensor [19]. After the conditioning process, the variations of the resonance frequency are directly linked to the concentration of ammonia. Where the water outflow causes a frequency shift of about 15 MHz, the frequency shift due to ammonia injections varies, depending on the concentration, from 1 to 3 MHz. This can be explained in part by the difference in the quantities involved. In the first case, it is a matter of a few tens or even hundreds of ppm of pollutant gas, whereas the water outflow corresponds to a stress of several million ppm.

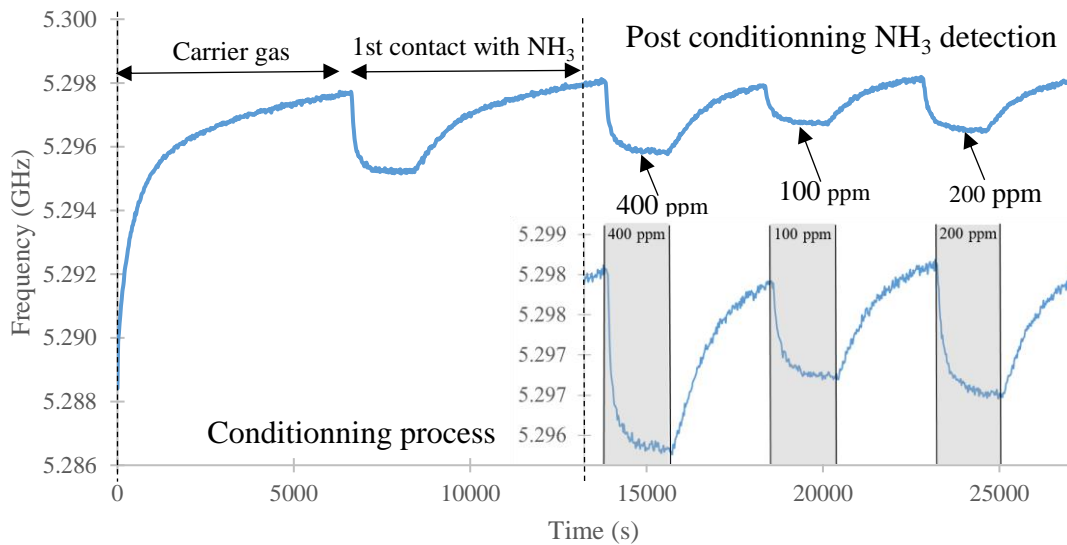


Fig. 5: Frequency shift during water desorption and ammonia injections at resonant frequency (5.29 GHz) vs time.

3.3 Comparison of regression models results to determine ammonia concentration

The regressors have been tested by considering only the magnitude or the phase response of the sensor in the dataset, however those results were found to be less relevant than taking into account both types of response at the same time. Therefore, only the results considering both types of sensor response are presented in this article.

In a first step, the used datasets consist of experimental data performed with a rectangular concentration profile. Indeed, the data from three different experiments (each of them done during a different day) are used as a training set and the data of another experiment (done during another day) as validation set. The training and validation sets are temporally distinct. Furthermore, a shuffle of the training set is done during runtime so that two consecutive time samples are not learned one after the other. This gives a training dataset of 2757 time samples and a validation dataset of 1367 time samples. The sensor used for these experiments have five frequencies of resonance.

Table 1 shows the different metrics results for each tested regressor. It can be observed that reducing the size of the data with PCA before applying a model on it does not improve the prediction of this models except the LR, and this despite components keeping 99% of the data variability. From the R^2 score it can be observed that a leading group stands out containing the CNN, MLP and RdmF, that the SVR and LR form the trailing group and that using Pearson's correlation as a feature selection diminish the quality of the results (with RdmF as an exception). Even though the CNN with manual selection has a R^2 score a bit inferior to the

RdmF with Pearson’s correlation, the CNN gives better results with a MAE of 34.05 ppm vs 35.14 ppm for the RdmF.

Table 1: Evaluation of the models applied to experimental data performed with a rectangular concentration profile.

	Manual		Pearson	
	MAE (ppm)	R ²	MAE (ppm)	R ²
PCA + SVR	62.72	0.2	61.21	0.16
SVR	62.96	0.18	60.68	0.17
PCA + KNN	65.69	0.41	71.69	-0.04
KNN	62.85	0.42	69.11	-0.08
PCA + RdmF	84.2	0.04	58.68	0.42
RdmF	37.43	0.79	35.14	0.83
PCA + LR	82.49	0.29	67.94	0.4
LR	171.45	-2.01	110.33	-0.23
PCA + MLP	90.98	-0.03	76.9	-0.08
MLP	39.69	0.73	64.51	0.22
CNN	34.05	0.79	60.44	0.35

Fig. 6 (a) represents the predictions made by the two best models for each time sample of an experiment. This shows that the better predictions are made without presence of pollutant. It can be assumed that that a bias is induce in the dataset because too much data is collected when no ammonia is present in the test chamber. It is probably this same bias that leads to poor results when using Pearson correlation for feature selection. Indeed, it can be seen in Fig. 6 (b), representing the prediction made by the model as function of the ground truth, that the CNN (orange) has a linear curve closer than the RdmF (in gray) to the line $y = x$. Better models would predict concentrations closer to the ground truth and therefore would have a scatter plot more concentrated around the line $y = x$, here in blue and labelled “y_true”. These results led to a reflection on the concentration profile used during the manipulations.

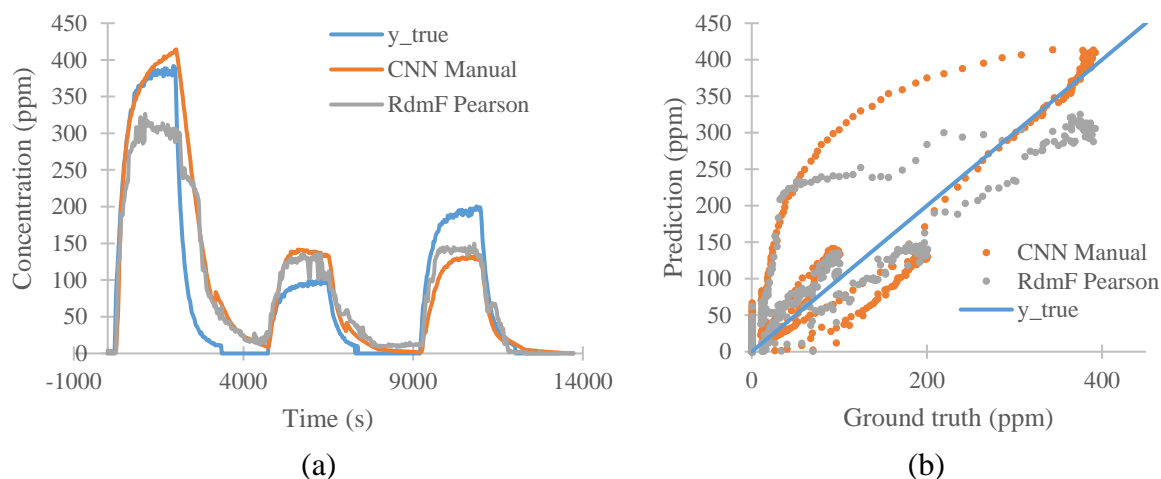


Fig. 6: (a) Predictions of the two best models for an experiment. (b) Prediction comparison of the two best models to the ground truth.

The type of profile describe so far is useful in laboratory to have a better understanding of the sensor or to simulate e-nose applications [52,53]. However, it does not simulate air quality monitoring in real conditions which are more random. Indeed, as show on Fig. 7 (a) this type of profile induces much return to zero (non-presence of pollutants). In order to have less biased results and a microwave response closer to real condition measurements a staircase kind of concentration profile is used on a second experiment campaign. This type of

concentration profile is composed of two parts. The first one is a period of sensor conditioning with 1 hour of dry air flow to eliminate water in the circuit followed by a 20 minutes of dry air flow with 400 ppm of ammonia and 20 minutes of air without pollutant. The second part is a period with a rise in 50 ppm steps and a fall in 50 ppm steps. These limits return to zero and gives a better balance in data representation (Fig. 7 (b)). To push the reflection and the limit of the chosen models even further a concentration profile used to generate validation data is designed (Fig. 7 (c)). Its objective is to have, after conditioning, a cycle with random concentration pulses. The staircase concentration profile induces a certain complexity in the data, if only because of the difference in the sensor response between the adsorption and desorption period [18]. Furthermore, the history of the sensor comes into play since there is no more period without pollutant between two concentration levels. However, this complexity is welcome because it induces physico-chemical phenomena that are closer to what will be found in real conditions of use of the sensor.

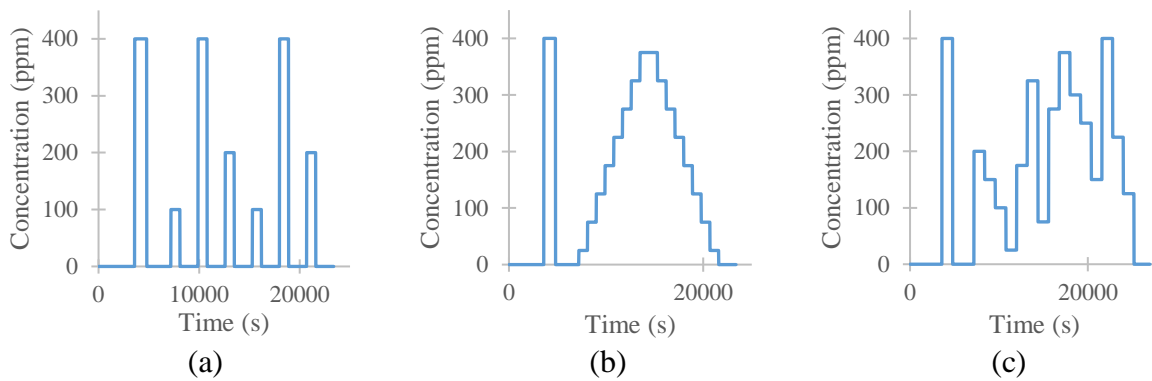


Fig. 7: (a) rectangular concentration profile; (b) staircase concentration profile for AI training; (c) concentration profile with random values without return to zero for AI validation.

The last six experiments of this new measurement campaign are dedicated to the development and training of the neural network. These experiments last about six to seven hours each and five of them are used for training the dataset for a total of 4597 time-samples and the last one for validation dataset for a total of 1072 time-samples.

Unlike before, here the use of Pearson improves the overall performance of the models compared to the manual selection of features. Indeed, Table 2 shows that SVR, RdmF and MLP models greatly benefit from it. However, this type of feature selection is not compatible with the CNN as a matter of fact its R^2 score goes from 0.82 to 0.32. Even if classical models give honorable performances the complexity of the problem makes the performances of the CNN and the MLP stand out ($R^2 > 0.80$). The MLP with Pearson gives the best metrics with a mean absolute error of 32.13 ppm (8%) over a range of 0 to 400 ppm of ammonia and R-squared score of 0.87.

Table 2: Evaluation metrics with datasets generated from simulated real conditions profiles

	Manual		Pearson	
	MAE (ppm)	R^2	MAE (ppm)	R^2
PCA + SVR	91.56	0.02	62.71	0.53
SVR	91.13	0.04	70.04	0.44
PCA + KNN	79.39	0.23	75.34	0.22
KNN	73.77	0.32	68.63	0.35
PCA + RdmF	81.54	0.17	71.73	0.36
RdmF	49.94	0.69	41.57	0.78
PCA + LR	79.81	0.32	64.96	0.55
LR	361.39	-10.63	417.54	-14.24
PCA + MLP	55.15	0.63	65.59	0.5

MLP	41.72	0.78	32.13	0.87
CNN	35.22	0.82	78.05	0.32

The evaluation of CNN with the manual feature selection give similar results with the two datasets but when we look at the CNN scatter plot of Fig. 6 (b) and Fig. 8 (b), we can see that the second dataset gives better predictions because they are less dispersed. This can imply that the second method of data generation is better for the presented regression problem.

Fig. 8 (a) plots the prediction obtained from the CNN with manual selection and MLP with Pearson selection for an experiment. The ground truth is in blue. They both overestimated the first concentrations but are overall rather reliable. The microwave response of this experiment is also overestimated on these first concentrations. This could be solved using a longer conditioning pulse.

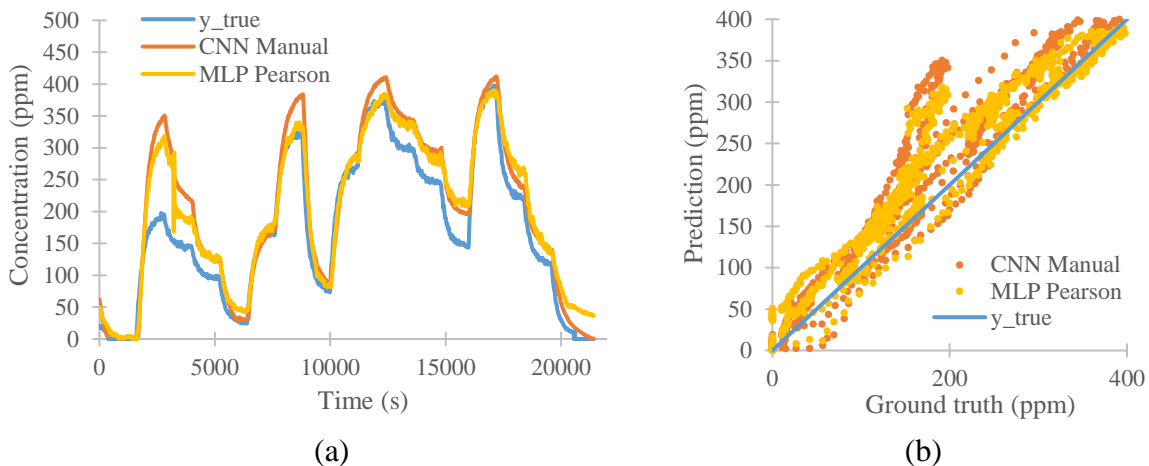


Fig. 8: (a) Prediction of CNN 6 inputs models for a validation dataset. (b) Prediction comparison of RF and CNN 6 inputs models.

4 Conclusion

The combination of the microwave response of the gas sensor presented with the interpretation of the mass spectrometer analyses resulted in the proposal of a protocol for a reasoned conditioning process to obtain qualitative and quantitative responses. The different steps of the conditioning process have been elaborated following the understanding of the role of water and of the surface phenomena involved during adsorption and desorption. The perspectives of this work from a physical chemistry point of view are the improvement of the microwave response at low concentration of ammonia (amplification process of the signal) and the reduction to the maximum of the remaining drift which however does not prevent the quantitative aspect of the response.

The combination of the microwave gas sensor with machine learning to determine the measured ammonia concentration is very promising. Different regression machine learning models and artificial neural networks are applied on time samples. The use of PCA for input data dimension reduction was inconclusive. To improve regression results, new concentration profiles are used to reduce biases induced by the presence of too much measurement obtained when no pollutant is present. The machine learning models applied to data obtained with the new concentration profiles give good results, and even more so with the use of Pearson's correlation for the feature selection. The MLP gives the best results with an average absolute error of 32.13 ppm (8%) over the range 0-400 ppm ammonia and an R-squared score of 0.87. Furthermore, with this model there is no need to consider the baseline of the sensor.

The perspectives of this work in machine learning are to be able to discriminate ammonia and water and to consider the history of the sensor (temporal analysis) to improve current results. In addition, the regression models used can be embedded in air pollution detection systems.

References

- [1] R. Cachon, P. Girardon, A. Voilley, *Gases in Agro-food Processes*, 1st Edition, 2019.
- [2] L. Engel, I. Benito-Altamirano, K.R. Tarantik, C. Pannek, M. Dold, J.D. Prades, J. Wöllenstein, Printed sensor labels for colorimetric detection of ammonia, formaldehyde and hydrogen sulfide from the ambient air, *Sensors and Actuators B: Chemical*. 330 (2021) 129281. <https://doi.org/10.1016/j.snb.2020.129281>.
- [3] B. Timmer, W. Olthuis, A. van den Berg, Ammonia sensors and their applications—a review, *Sensors and Actuators B: Chemical*. 107 (2005) 666–677. <https://doi.org/10.1016/j.snb.2004.11.054>.
- [4] B. Zhou, N. Zhang, Y. Wu, W. Yang, Y. Lu, Y. Wang, S. Wang, An option for green and sustainable future: Electrochemical conversion of ammonia into nitrogen, *Journal of Energy Chemistry*. 60 (2021) 384–402. <https://doi.org/10.1016/j.jechem.2021.01.011>.
- [5] D.A. Hauglustaine, Y. Balkanski, M. Schulz, A global model simulation of present and future nitrate aerosols and their direct radiative forcing of climate, *Atmospheric Chemistry and Physics*. 14 (2014) 11031–11063. <https://doi.org/10.5194/acp-14-11031-2014>.
- [6] C. Viatte, J.-E. Petit, S. Yamanouchi, M. van Damme, C. Doucerain, E. Germain-Piaulenne, V. Gros, O. Favez, L. Clarisse, P.-F. Coheur, K. Strong, C. Clerbaux, Ammonia and PM_{2.5} Air Pollution in Paris during the 2020 COVID Lockdown, *Atmosphere (Basel)*. 12 (2021) 160. <https://doi.org/10.3390/atmos12020160>.
- [7] T. Li, M. Zhou, Y. Qiu, J. Huang, Y. Wu, S. Zhang, H. Zhao, Membrane-based conductivity probe for real-time in-situ monitoring rice field ammonia volatilization, *Sensors and Actuators B: Chemical*. 286 (2019) 62–68. <https://doi.org/10.1016/j.snb.2019.01.099>.
- [8] C. Bernou, D. Rebière, J. Pistré, Microwave sensors: a new sensing principle. Application to humidity detection, *Sensors and Actuators B: Chemical*. 68 (2000) 88–93. [https://doi.org/10.1016/S0925-4005\(00\)00466-4](https://doi.org/10.1016/S0925-4005(00)00466-4).
- [9] E. Bou-Maroun, J. Rossignol, B. de Fonseca, C. Lafarge, R.D. Gougeon, D. Stuerger, P. Cayot, Feasibility of a microwave liquid sensor based on molecularly imprinted sol-gel polymer for the detection of iprodione fungicide, *Sensors and Actuators B: Chemical*. 244 (2017) 24–30. <https://doi.org/10.1016/J.SNB.2016.12.118>.
- [10] H. Hallil, P. Bahoumina, K. Pieper, J.L. Lachaud, D. Rebiere, A. Abdelghani, K. Frigui, S. Bila, D. Baillargeat, Q. Zhang, P. Coquet, E. Pichonat, H. Happy, C. Dejous, Differential passive microwave planar resonator-based sensor for chemical particle detection in polluted environments, *IEEE Sensors Journal*. 19 (2019) 1346–1353. <https://doi.org/10.1109/JSEN.2018.2881487>.

- [11] J. Jouhannaud, J. Rossignol, D. Stuerger, Développement d'un nouveau capteur de gaz basé sur la détection à large bande micro-onde, *Comptes Rendus Physique*. 8 (2007) 456–461. <https://doi.org/10.1016/J.CRHY.2007.04.013>.
- [12] J. Rossignol, P.D. Stuerger, Metal Oxide Nanoparticles Obtained by Microwave Synthesis and Application in Gas Sensing by Microwave Transduction, *Key Engineering Materials*. 605 (2014) 299–302. <https://doi.org/10.4028/WWW.SCIENTIFIC.NET/KEM.605.299>.
- [13] P. Bahoumina, H. Hallil, J.L. Lachaud, A. Abdelghani, K. Frigui, S. Bila, D. Baillargeat, A. Ravichandran, P. Coquet, C. Paragua, E. Pichonat, H. Happy, D. Rebière, C. Dejous, Microwave flexible gas sensor based on polymer multi wall carbon nanotubes sensitive layer, *Sensors and Actuators B: Chemical*. 249 (2017) 708–714. <https://doi.org/10.1016/J.SNB.2017.04.127>.
- [14] F. Li, Y. Zheng, C. Hua, J. Jian, Gas sensing by microwave transduction: Review of progress and challenges, *Frontiers in Materials*. 6 (2019) 101. <https://doi.org/10.3389/FMATS.2019.00101/BIBTEX>.
- [15] J. Rossignol, G. Barochi, B. de Fonseca, J. Brunet, M. Bouvet, A. Pauly, L. Markey, Microwave-based gas sensor with phthalocyanine film at room temperature, *Sensors and Actuators B: Chemical*. 189 (2013) 213–216. <https://doi.org/10.1016/J.SNB.2013.03.092>.
- [16] H. Hallil, C. Dejous, S. Hage-Ali, O. Elmazria, J. Rossignol, D. Stuerger, A. Talbi, A. Mazzamurro, P.Y. Joubert, E. Lefeuvre, Passive Resonant Sensors: Trends and Future Prospects, *IEEE Sensors Journal*. 21 (2021) 12618–12632. <https://doi.org/10.1109/JSEN.2021.3065734>.
- [17] B. de Fonseca, J. Rossignol, I. Bezverkhyy, J.P. Bellat, D. Stuerger, P. Pribetich, Detection of VOCs by microwave transduction using dealuminated faujasite DAY zeolites as gas sensitive materials, *Sensors and Actuators B: Chemical*. 213 (2015) 558–565. <https://doi.org/10.1016/J.SNB.2015.02.006>.
- [18] A. Lasserre, L. Grzelak, J. Rossignol, D. Stuerger, O. Brousse, P. Pribetich, M. Paindavoine, Influence of carrier gas on microwave gas response : Detection of ammonia in air / argon., in: *2020 IEEE SENSORS, 2020*: pp. 1–4. <https://doi.org/10.1109/SENSORS47125.2020.9278728>.
- [19] J. Rossignol, A. Harrabi, D. Stuerger, P. Pribetich, G. Bailly, T. Leblois, Critical Influence of Dielectric Sensitive Material and Manufactured Process in Microwave Gas-Sensing: Application of Ammonia Detection with an Interdigital Sensor, *ACS Omega*. 5 (2020) 11507–11514. <https://doi.org/10.1021/ACSOMEGA.0C00596>.
- [20] S. Reiß, D. Schönauer, G. Hagen, G. Fischerauer, R. Moos, Monitoring the Ammonia Loading of Zeolite-Based Ammonia SCR Catalysts by a Microwave Method, *Chemical Engineering & Technology*. 34 (2011) 791–796. <https://doi.org/10.1002/CEAT.201000546>.
- [21] A. Bogner, C. Steiner, S. Walter, J. Kita, G. Hagen, R. Moos, Planar Microstrip Ring Resonators for Microwave-Based Gas Sensing: Design Aspects and Initial Transducers

- for Humidity and Ammonia Sensing, *Sensors* 2017, Vol. 17, Page 2422. 17 (2017) 2422. <https://doi.org/10.3390/S17102422>.
- [22] J. Jun, J. Oh, D.H. Shin, S.G. Kim, J.S. Lee, W. Kim, J. Jang, Wireless, Room Temperature Volatile Organic Compound Sensor Based on Polypyrrole Nanoparticle Immobilized Ultrahigh Frequency Radio Frequency Identification Tag, *ACS Applied Materials and Interfaces*. 8 (2016) 33139–33147. https://doi.org/10.1021/ACSAMI.6B08344/ASSET/IMAGES/LARGE/AM-2016-08344V_0008.JPEG.
- [23] R.B. Vasiliev, M.N. Rumyantseva, L.I. Ryabova, B.A. Akimov, M. Labeau, M. Langlet, A.M. Gaskov, Memory effect and its switching by electric field in solid-state gas sensors, *Materials Science and Engineering: B*. 77 (2000) 106–109. [https://doi.org/10.1016/S0921-5107\(00\)00479-7](https://doi.org/10.1016/S0921-5107(00)00479-7).
- [24] M. Bendahan, P. Lauque, J.L. Seguin, K. Aguir, P. Knauth, Development of an ammonia gas sensor, *Sensors and Actuators B: Chemical*. 95 (2003) 170–176. [https://doi.org/10.1016/S0925-4005\(03\)00408-8](https://doi.org/10.1016/S0925-4005(03)00408-8).
- [25] T. Saidi, O. Zaim, M. Moufid, N. el Bari, R. Ionescu, B. Bouchikhi, Exhaled breath analysis using electronic nose and gas chromatography–mass spectrometry for non-invasive diagnosis of chronic kidney disease, diabetes mellitus and healthy subjects, *Sensors and Actuators B: Chemical*. 257 (2018) 178–188. <https://doi.org/10.1016/J.SNB.2017.10.178>.
- [26] M. Vinaixa, A. Vergara, C. Duran, E. Llobet, C. Badia, J. Brezmes, X. Vilanova, X. Correig, Fast detection of rancidity in potato crisps using e-noses based on mass spectrometry or gas sensors, *Sensors and Actuators B: Chemical*. 106 (2005) 67–75. <https://doi.org/10.1016/J.SNB.2004.05.038>.
- [27] D. Cozzolino, W. Cynkar, R. Damberg, P. Smith, Two-dimensional correlation analysis of the effect of temperature on the fingerprint of wines analysed by mass spectrometry electronic nose, *Sensors and Actuators B: Chemical*. 145 (2010) 628–634. <https://doi.org/10.1016/J.SNB.2010.01.003>.
- [28] S.K. Jha, Characterization of human body odor and identification of aldehydes using chemical sensor, *Reviews in Analytical Chemistry*. 36 (2017) 20160028. <https://doi.org/10.1515/REVAC-2016-0028/MACHINEREADABLECITATION/RIS>.
- [29] C. Li, G.W. Krewer, P. Ji, H. Scherm, S.J. Kays, Gas sensor array for blueberry fruit disease detection and classification, *Postharvest Biology and Technology*. 55 (2010) 144–149. <https://doi.org/10.1016/J.POSTHARVBIO.2009.11.004>.
- [30] M. Barriault, I. Alexander, N. Tasnim, A. O'Brien, H. Najjaran, M. Hoorfar, Classification and Regression of Binary Hydrocarbon Mixtures using Single Metal Oxide Semiconductor Sensor With Application to Natural Gas Detection, *Sensors and Actuators B: Chemical*. 326 (2021) 129012. <https://doi.org/10.1016/J.SNB.2020.129012>.
- [31] J.S. Cooper, H. Kiiveri, E. Chow, L.J. Hubble, M.S. Webster, K.H. Müller, B. Raguse, L. Wiczorek, Quantifying mixtures of hydrocarbons dissolved in water with a partially

- selective sensor array using random forests analysis, *Sensors and Actuators B: Chemical*. 202 (2014) 279–285. <https://doi.org/10.1016/J.SNB.2014.05.094>.
- [32] H. Ji, W. Qin, Z. Yuan, F. Meng, Qualitative and quantitative recognition method of drug-producing chemicals based on SnO₂ gas sensor with dynamic measurement and PCA weak separation, *Sensors and Actuators B: Chemical*. 348 (2021) 130698. <https://doi.org/10.1016/J.SNB.2021.130698>.
- [33] E.M. Taguem, L. Mennicken, A.C. Romain, Quantile regression with a metal oxide sensors array for methane prediction over a municipal solid waste treatment plant, *Sensors and Actuators B: Chemical*. 334 (2021) 129590. <https://doi.org/10.1016/J.SNB.2021.129590>.
- [34] J. Fonollosa, S. Sheik, R. Huerta, S. Marco, Reservoir computing compensates slow response of chemosensor arrays exposed to fast varying gas concentrations in continuous monitoring, *Sensors and Actuators B: Chemical*. 215 (2015) 618–629. <https://doi.org/10.1016/J.SNB.2015.03.028>.
- [35] X. Pan, Z. Zhang, H. Zhang, Z. Wen, W. Ye, Y. Yang, J. Ma, X. Zhao, A fast and robust mixture gases identification and concentration detection algorithm based on attention mechanism equipped recurrent neural network with double loss function, *Sensors and Actuators B: Chemical*. 342 (2021) 129982. <https://doi.org/10.1016/J.SNB.2021.129982>.
- [36] S. Qiu, J. Wang, C. Tang, D. Du, Comparison of ELM, RF, and SVM on E-nose and E-tongue to trace the quality status of mandarin (Citrus unshiu Marc.), *Journal of Food Engineering*. 166 (2015) 193–203. <https://doi.org/10.1016/J.JFOODENG.2015.06.007>.
- [37] G. Bailly, A. Harrabi, J. Rossignol, M. Michel, D. Stuerger, P. Pribetich, Microstrip Spiral Resonator For Microwave-Based Gas Sensing, *IEEE Sensors Letters*. 1 (2017) 1–4. <https://doi.org/10.1109/LESENS.2017.2716413>.
- [38] J.B. Westmore, M.M. Alauddin, Ammonia chemical ionization mass spectrometry, *Mass Spectrometry Reviews*. 5 (1986) 381–465. <https://doi.org/10.1002/MAS.1280050403>.
- [39] F. Arena, R. di Chio, G. Trunfio, An experimental assessment of the ammonia temperature programmed desorption method for probing the surface acidic properties of heterogeneous catalysts, *Applied Catalysis A: General*. 503 (2015) 227–236. <https://doi.org/10.1016/J.APCATA.2015.05.035>.
- [40] J. Benesty, J. Chen, Y. Huang, I. Cohen, Pearson correlation coefficient, *Springer Topics in Signal Processing*. 2 (2009) 1–4. https://doi.org/10.1007/978-3-642-00296-0_5.
- [41] I. Jolliffe, Principal Component Analysis, *Encyclopedia of Statistics in Behavioral Science*. (2005). <https://doi.org/10.1002/0470013192.BSA501>.
- [42] K.C. Lin, T.Y. Liu, P.H. Chen, C.T. Lin, Use Support Vector Machine (SVM) to estimate gas concentration in mixture condition, *Proceedings of the 2017 IEEE International Conference on Applied System Innovation: Applied System Innovation*

- for Modern Technology, ICASI 2017. (2017) 744–746.
<https://doi.org/10.1109/ICASI.2017.7988537>.
- [43] A. Roncaglia, I. Elmi, L. Dori, M. Rudan, Adaptive K-NN for the Detection of Air Pollutants With a Sensor Array, *IEEE Sensors Journal*. 4 (2004) 248–256.
<https://doi.org/10.1109/JSEN.2004.823653>.
- [44] S. Acharyya, B. Jana, S. Nag, G. Saha, P.K. Guha, Single resistive sensor for selective detection of multiple VOCs employing SnO₂ hollowspheres and machine learning algorithm: A proof of concept, *Sensors and Actuators B: Chemical*. 321 (2020) 128484.
<https://doi.org/10.1016/J.SNB.2020.128484>.
- [45] H. Abdi, The method of least squares, *Encyclopedia of Measurement and Statistics*. (2007).
<https://citeseerx.ist.psu.edu/viewdoc/download?doi=10.1.1.450.6396&rep=rep1&type=pdf> (accessed November 16, 2021).
- [46] H. Drucker, C.J. Burges, L. Kaufman, A. Smola, V. Vapnik, Support Vector Regression Machines, *Adv Neural Inf Process Syst*. 9 (1997) 155–161.
<https://www.researchgate.net/publication/2378203> (accessed November 16, 2021).
- [47] M. Awad, R. Khanna, Support Vector Regression, *Efficient Learning Machines*. (2015) 67–80. https://doi.org/10.1007/978-1-4302-5990-9_4.
- [48] D.P. Kingma, J.L. Ba, Adam: A Method for Stochastic Optimization, 3rd International Conference on Learning Representations, ICLR 2015 - Conference Track Proceedings. (2014). <https://arxiv.org/abs/1412.6980v9> (accessed December 10, 2021).
- [49] A. Botchkarev, Performance Metrics (Error Measures) in Machine Learning Regression, Forecasting and Prognostics: Properties and Typology, *Interdisciplinary Journal of Information, Knowledge, and Management*. 14 (2018) 45–76.
<https://doi.org/10.28945/4184>.
- [50] D. Chicco, M.J. Warrens, G. Jurman, The coefficient of determination R-squared is more informative than SMAPE, MAE, MAPE, MSE and RMSE in regression analysis evaluation, *PeerJ Computer Science*. 7 (2021) 1–24. <https://doi.org/10.7717/PEERJ-CS.623/SUPP-1>.
- [51] G. Bailly, J. Rossignol, D. Stuerger, P. Pribetich, B. Domenichini, NAP-XPS Study of Ethanol Adsorption on TiO₂ Surfaces and Its Impact on Microwave-Based Gas Sensors Response, *Proc West Mark Ed Assoc Conf*. 1 (2017) 416.
<https://doi.org/10.3390/proceedings1040416>.
- [52] J. Zhang, Y. Xue, Q. Sun, T. Zhang, Y. Chen, W. Yu, Y. Xiong, X. Wei, G. Yu, H. Wan, P. Wang, A miniaturized electronic nose with artificial neural network for anti-interference detection of mixed indoor hazardous gases, *Sensors and Actuators B: Chemical*. 326 (2021) 128822. <https://doi.org/10.1016/J.SNB.2020.128822>.
- [53] T. Wang, H. Zhang, Y. Wu, W. Jiang, X. Chen, M. Zeng, J. Yang, Y. Su, N. Hu, Z. Yang, Target discrimination, concentration prediction, and status judgment of electronic nose system based on large-scale measurement and multi-task deep learning,

Sensors and Actuators B: Chemical. 351 (2022) 130915.
<https://doi.org/10.1016/J.SNB.2021.130915>.

Appendix

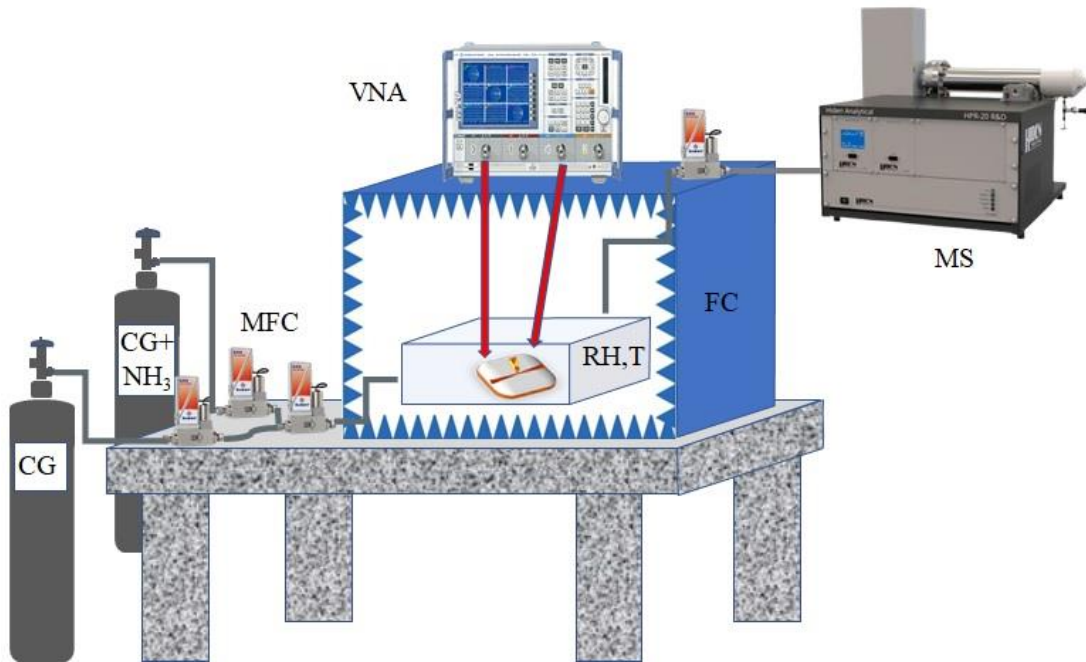


Fig. A.1. Test bench as described in Material and Method part of the article. (VNA = Vector Network Analyzer, CG = Carrier Gas, MFC = Mass Flow Controller, RH = Relative Humidity sensor, T = Temperature sensor, FC = Faraday Cage, MS = Mass Spectrometer)

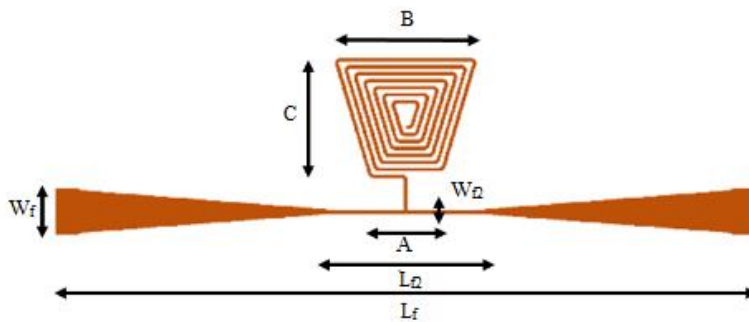


Fig. A.2. Resonator structure and its dimensions. $W_f = 2$ mm, $W_{f2} = 0.150$ mm, $L_f = 30$ mm, $L_{f2} = 6$ mm, $A = 3$ mm, $B = 6$ mm, $C = 5$ mm, number of coils = 7, coils width = 0.150 mm, coils spacing = 0.150 mm

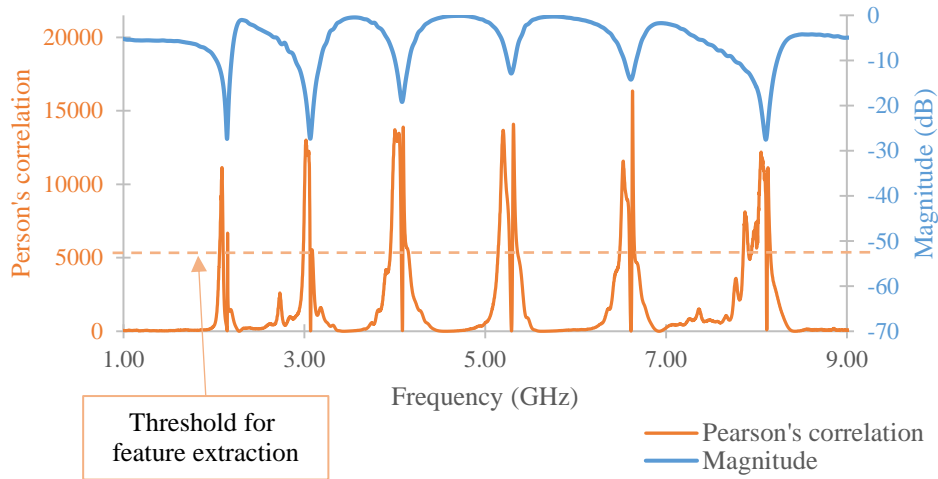


Fig. A.3. Example of feature extraction with Pearson's correlation (orange) vs magnitude (blue) as function of frequency.

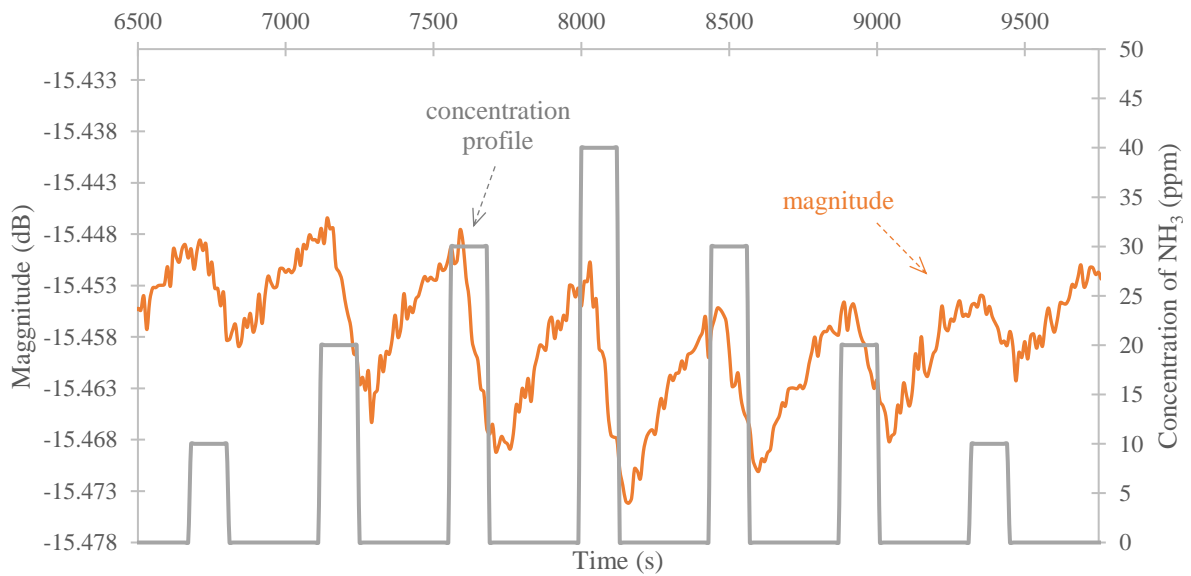


Fig. A.4. Magnitude at resonant frequency (at 6.70 GHz, in orange) and concentration profile (in gray) vs time for low ammonia concentrations (10 to 40 ppm).